Journal of Power Sources 197 (2012) 325–329

Contents lists available at SciVerse ScienceDirect

Journal of Power Sources

journal homepage: www.elsevier.com/locate/jpowsour

Short communication

Three-dimensional bicontinuous nanoporous Au/polyaniline hybrid films for high-performance electrochemical supercapacitors

Xingyou Lang[a,b], Ling Zhang[a], Takeshi Fujita[a], Yi Ding[c], Mingwei Chen[a,d,*]

[a] WPI Advanced Institute for Materials Research, Tohoku University, Sendai 980-8577, Japan
[b] Key Laboratory of Automobile Materials (Jilin University), Ministry of Education, School of Materials Science and Engineering, Jilin University, Changchun 130022, PR China
[c] School of Chemistry and Chemical Engineering, Shandong University, Jinan 250100, PR China
[d] State Key Laboratory of Metal Matrix Composites, School of Materials Science and Engineering, Shanghai Jiaotong University, Shanghai 200030, PR China

ARTICLE INFO

Article history:
Received 15 July 2011
Accepted 3 September 2011
Available online 8 September 2011

Keywords:
Hybrid materials
Nanoporous metal
Polyaniline
Capacitors
Supercapacitors

ABSTRACT

We report three-dimensional bicontinuous nanoporous Au/polyaniline (PANI) composite films made by one-step electrochemical polymerization of PANI shell onto dealloyed nanoporous gold (NPG) skeletons for the applications in electrochemical supercapacitors. The NPG/PANI based supercapacitors exhibit ultrahigh volumetric capacitance (~1500 F cm^{-3}) and energy density (~0.078 Wh cm^{-3}), which are seven and four orders of magnitude higher than these of electrolytic capacitors, with the same power density up to ~190 W cm^{-3}. The outstanding capacitive performances result from a novel nanoarchitecture in which pseudocapacitive PANI shells are incorporated into pore channels of highly conductive NPG, making them promising candidates as electrode materials in supercapacitor devices combing high-energy storage densities with high-power delivery.

Growing concerns about environmental problems and upcoming depletion of fossil fuels have stimulated intense research on alternative electrochemical energy storage and conversion systems including batteries, fuel cells, and supercapacitors [1–3]. Among them, electrochemical supercapacitors (SCs) have attracted much attention because of their unique high-power performance associated with moderate energy density and long lifetime [4,5], which bridges the gap between these of batteries [1,6] and conventional electrolytic capacitors [4,5]. While typical electric double-layer SCs based on carbon in various forms [7–11] and metal electrode materials [12], storing charges with ultrafast charge/discharge rates by making use of nonFaradic surface ion adsorption and enhancing ion and electron transports [4,5,7–13], are ideal for applications that require short-term power boosts [4,5,13], they only offer the energy densities measured in specific capacitance on the order of ~100 F cm^{-3} [14,15]. To circumvent the key limitation of conventional electrochemical double-layer capacitors with low energy density, great efforts have been devoted on pseudocapacitive materials like conducting polymers [16–19] and transition metal oxides [20–24], where the mechanism of fast and Faradic surface redox reaction offers the high energy storage [4,5,25], complementing or even replacing batteries. Polyaniline (PANI) is generally considered to be the most promising conducting polymers for the next generation of SC devices because of its high-energy density owing to multiple redox states and excellent environmental stability as well as low cost [19,26,27]. Although a nanoscale approach addressing the issue of ion transport in electrodes could improve the capacitive performance [28,29], the low conductivity of PNAI (~10^{-10} or ~1 S cm^{-1} for undoped or doped state) in various nanostructures [26–29] fabricated by chemical or electrochemical polymerization cannot satisfy another important requirement, i.e., high electron transport in electrodes, for high-power performance of electrical energy storage devices [30–32]. This essentially limits the widespread and practical uses of PANI based SCs. Here we show three-dimensional (3D) bicontinuous nanoporous Au/PANI hybrid films fabricated by electrochemical polymerization for the high power- as well as high energy-density SC applications. The free-standing and flexible composite films yield a volumetric capacitance up to ~1500 F cm^{-3}, 10 times higher than that of graphene/PANI composites (~150 F cm^{-3}), as a result of the concurrently enhanced ion and electron transports due to the intimate interaction and synergetic effect of highly conductive bicontinuous Au skeleton and pseudocapacitive PANI shells.

The fabrication of nanoporous Au/PANI composite films was accomplished by electrochemical polymerization of aniline occurring on the internal surface of 3D nanoporous gold (NPG) films using potentiodynamic method in a classic three-electrode setup (Fig. 1a, also *see* Method in Supporting Information for details).

* Corresponding author at: WPI Advanced Institute for Materials Research, Tohoku University, Sendai 980-8577, Japan. Tel.: +81 22 217 5959; fax: +81 22 217 5955.
E-mail address: mwchen@wpi-aimr.tohoku.ac.jp (M. W. Chen).

0378-7753/$ – see front matter © 2011 Elsevier B.V. All rights reserved.
doi:10.1016/j.jpowsour.2011.09.006

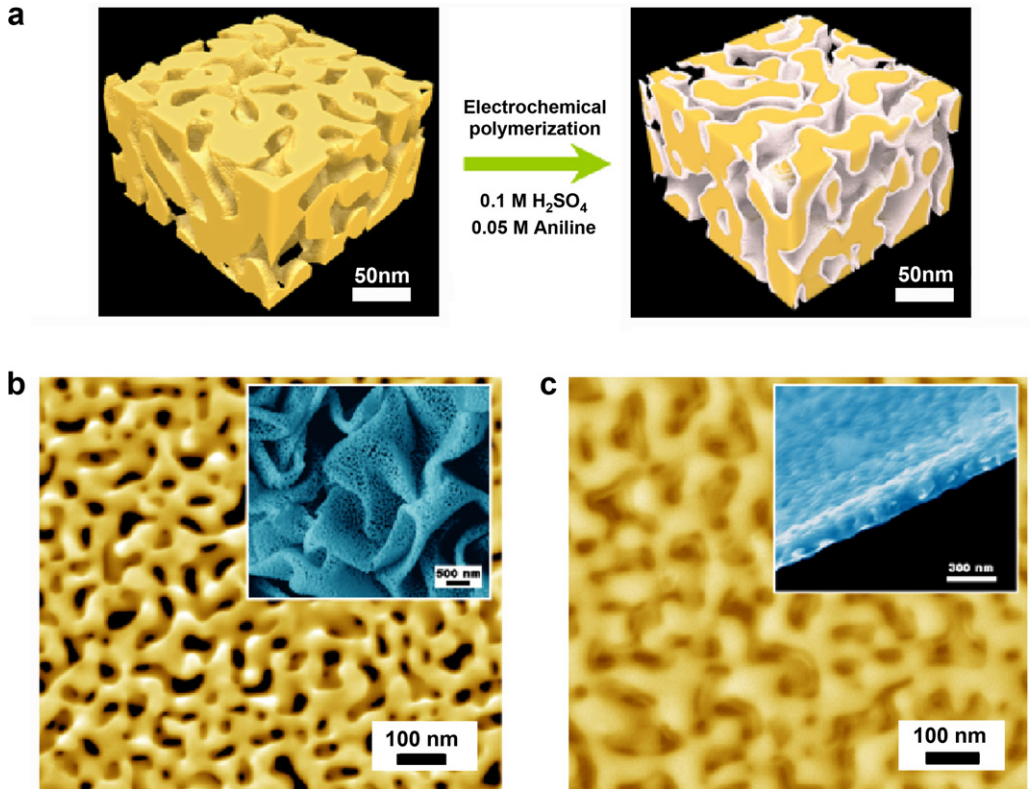

Fig. 1. (a) Schematic diagram showing the fabrication of 3D nanoporous Au/PANI composite films by electrochemical polymerization. (b) SEM image of nanoporous gold dealloyed for 8 h in HNO_3. Inset: the wrinkled films illustrating that nanoporous gold films exhibit excellent flexibility. (c) Typical top-view and cross-section (inset) SEM micrographs of nanoporous Au/PANI composite films electroplated for 10-cycle plating.

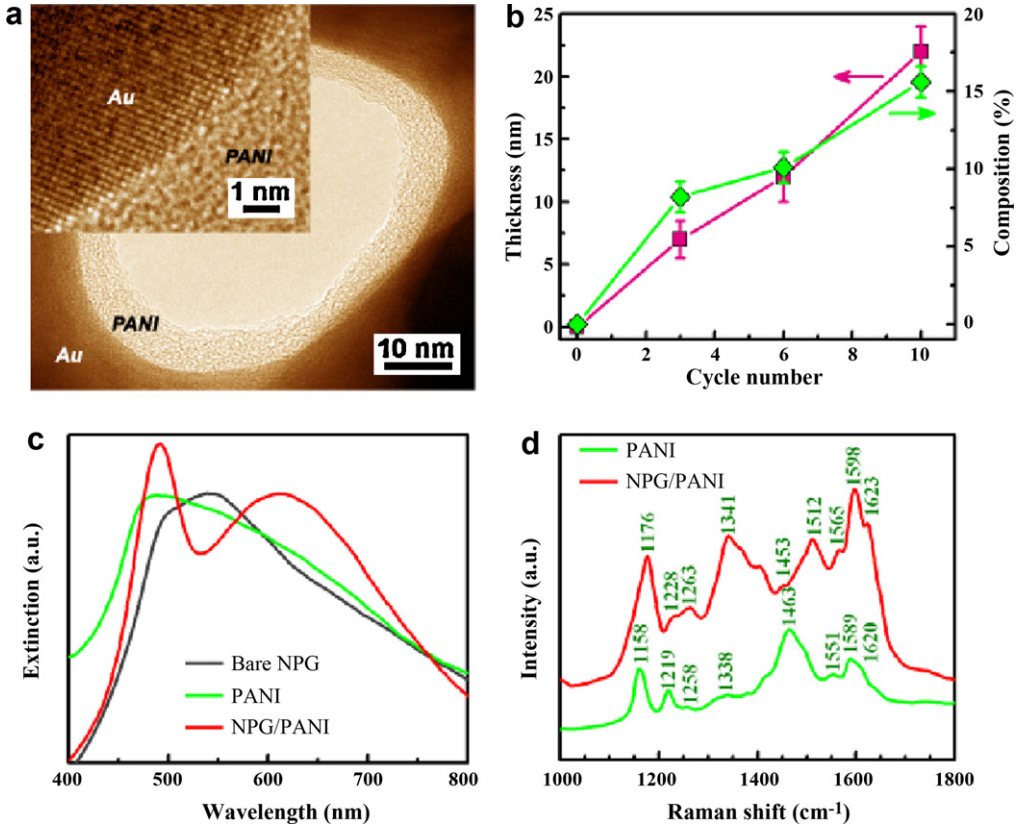

Fig. 2. (a) Representative TEM micrograph of nanoporous Au/PANI composite electroplated for 3-cycle electroplating. Inset: high resolution TEM image of Au/PAIN interface. (b) Thickness of PANI shells associated with volume fraction as a function of the cycle number of electrochemical polymerization. (c) UV–vis extinction and (d) Raman spectra of as-dealloyed NPG, PANI, and nanoporous Au/PANI composite films.

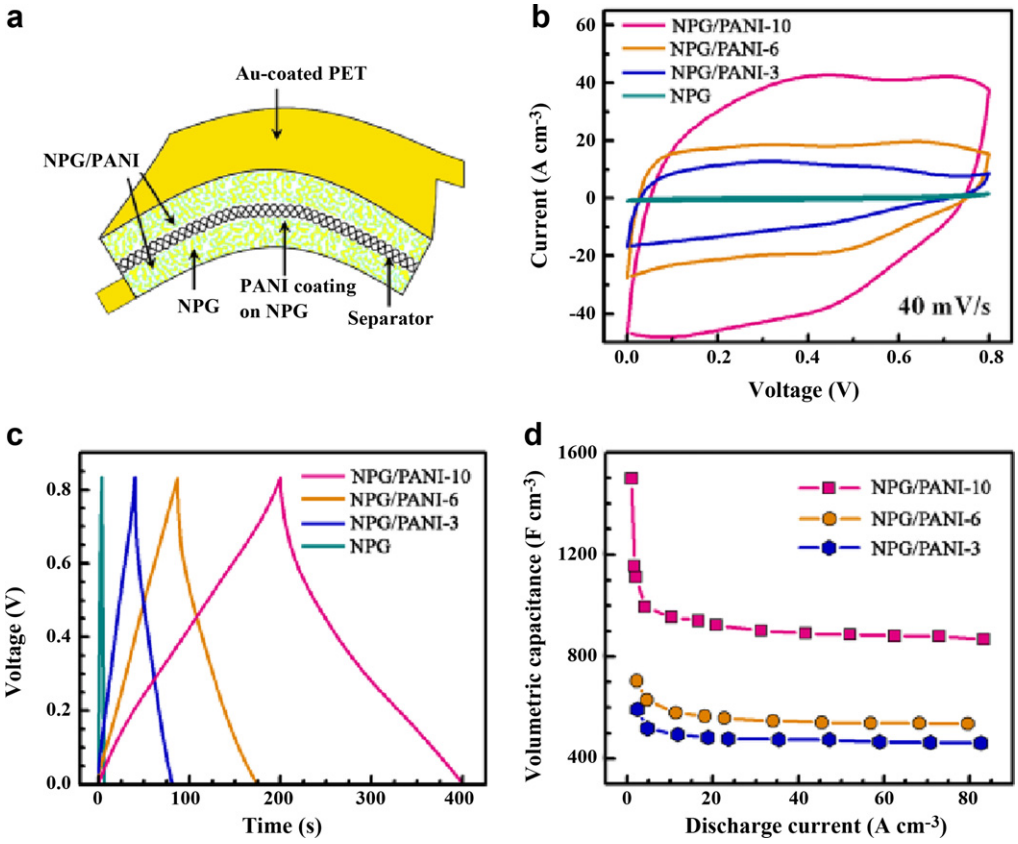

Fig. 3. (a) Configuration of the highly flexible supercapacitors based on nanoporous Au/PANI composite films. (b) Cyclic voltammograms at the scan rate of 40 mV s^{-1} and (c) galvanostatic charge/discharge curves at 4.2 A cm^{-3} for supercapacitors based on the electrodes of bare NPG and nanoporous Au/PANI with different compositions. (d) Volumetric capacitance of bare NPG and nanoporous Au/PANI composites as a function of discharge current density. The electrolyte is the 1 M $HClO_4$ solution.

The NPG films used in this work were prepared by chemically dealloying $Ag_{65}Au_{35}$ (at.%) leaves in concentrated HNO_3 for 8 h, during which less noble Ag is selectively dissolved while remained Au forms a open and bicontinuous nanoporous structure consisting of quasi-periodic gold ligaments and nanopore channels with the characteristic length of ~30–40 nm (Fig. 1b) [12,33]. The unique nanoarchitecture enables NPG films to simultaneously exhibit ultrahigh electrical conductivity up to 1.85×10^5 S cm^{-1} at room temperature (Fig. 1S, in Supporting Information) as well as good flexibility, as illustrated by the scanning electron microscope (SEM) micrograph (inset of Fig. 1b) of the wrinkled specimen produced by thermal contraction of an underlying pre-strained polystyrene substrate, where the gold ligaments do not break even with the curvature radius of tens nanometers [34]. Meanwhile, the pore channels in NPG allow aniline monomers to diffuse into the whole film and be polymerized to PANI to coat on the internal surface. Fig. 1c shows a typical top-view SEM image of nanoporous Au/PANI after electrochemical polymerization, clearly demonstrating the uniform coating of PANI and the good maintenance of 3D bicontinuous nanoporosity (*see* the cross-section SEM image in the inset of Fig. 1c). This is further verified by representative bright-field transmission electron microscope (TEM) micrographs shown in Figs. 2 and 2S for nanoporous Au/PANI composites with different volume fractions that were precisely tuned by adjusting the number of sweeping cycles during the potentiodynamic polymerization (Fig. 2b). The hybrid nanostructure can be clearly identified by the contrast between the bright PANI shell and the dark gold skeleton. Interfacial analysis revealed by high-resolution TEM (inset of Fig. 2a) demonstrates the intimate interaction between Au and PANI *via* the formation of chemical bonds. This unique interfacial structure ensures the occurrence of the PANI/Au charge transfer, verified by the UV–visible (UV–vis) extinction spectrum and Raman spectrum of nanoporous Au/PANI. In the UV–vis spectrum displayed in Fig. 2c, the buildup of polarization charges on the dielectric side of the interface gives rise to the noticeable red shift of localized surface plasmon (LSP) peak of nanoporous Au/PANI composite film in comparison with that of bare NPG and PANI films, and the LSP resonance shifts to longer wavelength as the thickness of PANI layer is increased (Fig. 3S) [35]. Raman spectrum of nanoporous Au/PANI collected under the excitation of 632.8 nm laser is presented in Fig. 2d. The Raman peaks of PANI shift slightly to the higher frequency after combined with NPG, suggesting that chemical reactions take place at polymer/metal interface [36]. These fascinating structural properties enable nanoporous Au/PANI films to exhibit two advantages for enhancing ion and electron transport kinetics in the nanocomposite electrode materials: (i) well interconnected porous channels not only allow rapid ion transport in the electrodes but also provide extremely large specific surface area of electrode/electrolyte interface, facilitating the full use of large pseudocapacitance of PANI; (ii) the bicontinuous Au network with ultrahigh electrical conductivity and the excellent contact between PANI and Au ligaments assists the fast electron transport in electrodes, as proved by the low internal resistance in the electrode assembly (Fig. 4S).

Electrochemical performances of the nanoporous Au/PANI electrodes were measured based on a two-electrode SC device (Fig. 3a), which was constructed with two nanoporous Au/PANI composite films as both electrodes and current collectors and one piece of cotton paper as a separator. In a 1 M $HClO_4$ aqueous electrolyte, the cyclic voltammograms (CVs) of the nanoporous Au/PANI composite

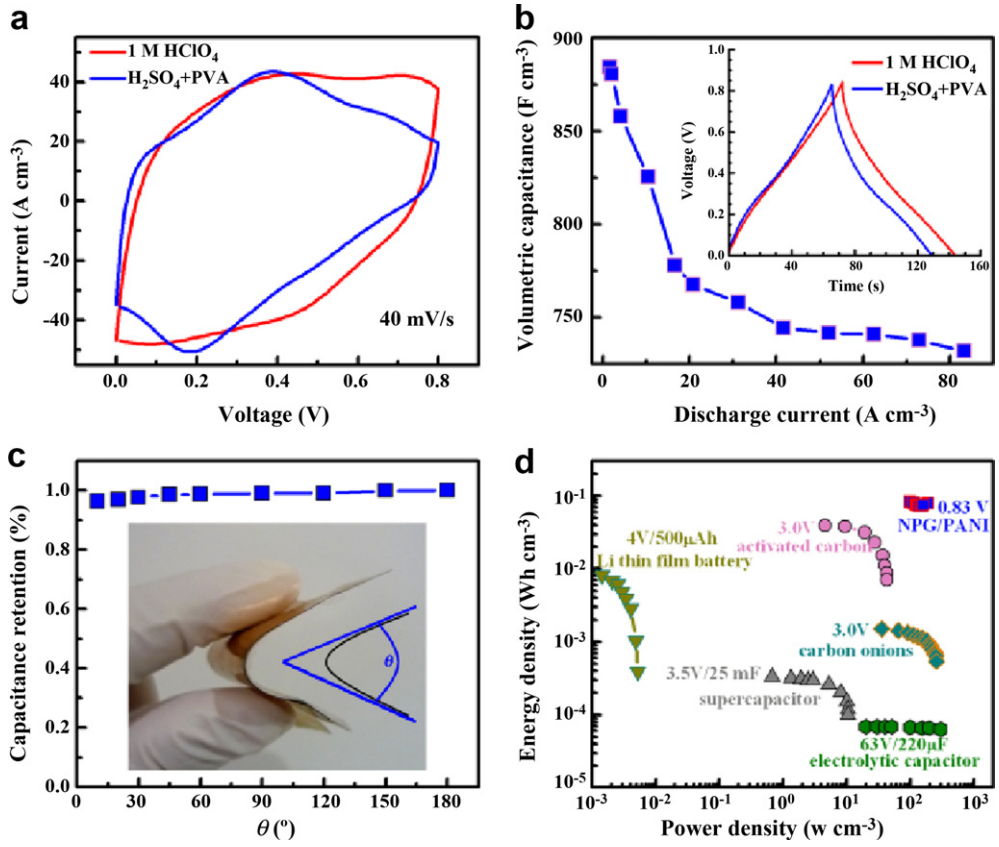

Fig. 4. Electrochemical performances of all-solid-state supercapacitor based on nanoporous Au/PANI composite with 10-cycle electrochemical polymerization. (a) Comparison of cyclic voltammograms of supercapacitors devices in the H_2SO_4-PVA gel electrolyte and 1 M $HClO_4$ solution. The scan rate is 40 mV s^{-1}. (b) Volumetric capacitance as a function of discharge current. Inset: the voltage–time profiles of nanoporous Au/PANI supercapacitors in the H_2SO_4-PVA gel electrolyte and 1 M $HClO_4$ solution. (c) Bend-angle dependence of capacitance retention. Inset: digital picture showing all-solid-state devices with excellent flexibility. (d) Ragone plot comparing the power and energy densities of the all-solid-state nanoporous Au/PANI supercapacitor to the reported values of carbon-based ones [8].

electrodes as a function of cycling number of potentiodynamic polymerization at the scan rate of 40 mV s^{-1} are shown in Fig. 3b. The redox peaks associated with much higher current densities than that of bare NPG based SC indicate the presence of pseudocapacitance from PANI, on which the energy storage and delivery are realized by Faradic redox reaction accompanied by leucoemeraldine/emeraldine and emeraldine/pemigraniline structural conversions [26,27,31]. Fig. 3c displays the representative galvanostatic charge/discharge curves of nanoporous Au/PANI based SC devices at the current density of 4.2 A cm^{-3}, demonstrating that the discharge time of the SC based on the nanoporous Au/PANI composite with 10-cycle plating is much longer than these of ones based on bare NPG as well as nanoporous Au/PANI films with 3- and 6-cycle plating. In comparison with the triangular-shape of the voltage–time profile of the pure NPG based SC with double-layer capacitance, the discharge curves of nanoporous Au/PANI based SCs consist of two voltage stages: one is in the range of 0 to ~0.7 V with much longer discharging duration contributed from both double-layer capacitance and Faradic pseudocapacitance of nanoporous Au/PANI composite; the other is the stage of ~0.7 to ~0.83 V with short discharging duration as a result of the double-layer capacitive behavior of porous nanostructure [31]. The increases of current densities in CVs and discharge times with the increasing cycling number of electrochemical polymerization reveal the strong dependence of capacitive behavior of the nanoporous Au/PANI electrodes on the loading amount of PANI as well as the nanoporosity, as shown in Fig. 3d that plots the volumetric capacitances (C_v) of nanoporous Au/PANI composite electrodes as a function of applied current densities. Here C_v is calculated according to the charge/discharge curves, $C_v = i/[-(\Delta V/\Delta t)v]$, with i being the applied current, $-\Delta V/\Delta t$ the slope of the discharge curve after the voltage drop at the beginning of each discharge, and v the volume of composite electrode. As shown in this plot, the nanoporous Au/PANI film with 10-cycle plating exhibits a volumetric capacitance up to ~1500 F cm^{-3} at the current density of ~1 A cm^{-3}. Even the current density is increased to ~80 A cm^{-3}, the composite electrode maintains the volumetric capacitance of ~866 F cm^{-3}, which is much higher than these of graphene/PANI composites (135 [30] and 160 F cm^{-3} [31]), as well as carbon/MnO_2 electrodes (156 F cm^{-3}) at 0.4 A cm^{-3} [37], and the layer-by-layer-assembled MWNT/MnO_2 electrode (246 F cm^{-3}) at 1.8 A cm^{-3} [23].

In view of the structural and chemical stability, the all-solid-state SC based on nanoporous Au/PANI with 10-cycle plating was assembled by using a gel electrolyte consisting of H_2SO_4 and polyvinyl alcohol (PVA) (see the Method for details) [38]. CV (Fig. 4a) and galvanostatic charge/discharge (inset of Fig. 4b) measurements carried out at room temperature demonstrate that the all-solid-state device has the capacitive performance comparable to the one in 1 $HClO_4$ solution. In spite of the slightly lower volumetric capacitance possibly due to the lower ionic mobility of gel electrolyte, the all-solid-state SC has a smaller capacitance decay (~18%) compared with the aqueous one (43%) as the discharge current densities decreases from ~1 to 80 A cm^{-3} (Figs. 3d and 4b). Moreover, the entire all-solid-state device exhibits the superior mechanical flexibility (inset of Fig. 4c). As shown in Fig. 4c, the macroscopic bend of the all-solid-state device from 180 to 10°

does not remarkably influence and capacitance retention. Fig. 4d presents the volumetric Ragone plot (power density P vs. energy density E) of the all-solid-state SC device, wherein the volumetric P and E are calculated by $P = V^2/(4Rv)$ and $E = 0.5CV^2/v$, respectively. Here V is the cutoff voltage, C is the measured device capacitance, and $R = \Delta V_{IR}/(2i)$ with ΔV_{IR} being the voltage drop between the first two points in the voltage drop at its top cutoff. The location of power and energy densities at the up-right region in the Ragone plot demonstrates the outstanding performance of the SC device based on nanoporous Au/PANI composite electrodes compared with other energy storage devices, such as SCs based on carbon onion and activated carbon, as well as a 500 μA h thin film lithium ion battery (LIB) and an electrolytic capacitor [8]. As we can see, the all-solid-state device has the energy density of ~0.078 Wh cm^{-3}, which is 10^4 times higher than that of conventional electrolytic capacitor with the similar a power density [8], and the maximum power density up to ~190 W cm^{-3}, which is ~3.6×10^4 folds higher than that of thin film LIB with the maximum energy density of ~0.0081 Wh cm^{-3} [8].

In summary, we have fabricated 3D bicontinuous nanoporous Au/PANI composite electrodes, and demonstrated the free-standing composite films as a promising electrode material for high-performance aqueous and all-solid-state supercapacitors with ultrahigh power density, high energy density. The good capacitive behaviors of the nanoporous Au/PANI SC devices arise from the ion and electron transports enhanced by unique bicontinuous nanostructure, where the nanoporosity facilitates the fast ion diffusion, and provides the large PANI/electrolyte interface to ensure the sufficient redox reaction of PANI during charge/discharge processes, and the 3D interconnected Au network with ultrahigh electrical conductivity harnesses the electron transport by remarkably decreasing the internal resistance of assembled devices.

Acknowledgements

This work was sponsored by Global COE for Materials Research and Education, the Ministry of Education, Culture, Sports, Science and Technology (MEXT), Japan, and Program for New Century Excellent Talents in University, the Ministry of Education, China.

Appendix A. Supplementary data

Supplementary data associated with this article can be found, in the online version, at doi:10.1016/j.jpowsour.2011.09.006.

References

[1] M. Winter, R.J. Brodd, Chem. Rev. 104 (2004) 4245–4269.
[2] A.S. Aricò, P. Bruce, B. Scrosati, J. Tarascon, W. van Schalkwijk, Nat. Mater. 4 (2005) 366–377.
[3] C. Liu, F. Li, L.P. Ma, H.M. Cheng, Adv. Mater. 22 (2010) E28–E62.
[4] P. Simon, Y. Gogotsi, Nat. Mater. 7 (2008) 845–854.
[5] B.E. Conway, Electrochemical Supercapacitors: Scientific Fundamentals and Technological Applications, Kluwer, 1999.
[6] P.G. Bruce, B. Scrosati, J.M. Tarascon, Angew. Chem. Int. Ed. 47 (2008) 2930–2946.
[7] M. Kaempgen, C.K. Chan, J. Ma, Y. Cui, G. Gruner, Nano Letters 9 (2009) 1872–1876.
[8] D. Pech, M. Brunet, H. Durou, P.H. Huang, V. Mochalin, Y. Gogotsi, P.L. Taberna, P. Simon, Nat. Nanotechnol. 5 (2010) 651–654.
[9] J. Chmiola, C. Largeot, P.L. Taberna, P. Simon, Y. Gogotsi, Science 328 (2010) 480–483.
[10] J.R. Miller, R.A. Outlaw, B.C. Holloway, Science 329 (2010) 1637–1639.
[11] V.L. Pushparaj, M.M. Shaijumon, A. Kumar, S. Murugesan, L.J. Ci, R. Vajtai, R.J. Linhardt, O. Nalamasu, P.M. Ajayan, Proc. Natl. Acad. Sci. U.S.A. 104 (2007) 13574–13577.
[12] X.Y. Lang, H.T. Yuan, Y. Iwasa, M.W. Chen, Scripta Mater. 64 (2011) 923–926.
[13] J.R. Miller, P. Simon, Science 321 (2008) 651–652.
[14] E. Frackowiak, F. Béguin, Carbon 39 (2001) 937–950.
[15] Y.J. Kim, Y. Abe, T. Yanagiura, K.C. Park, M. Shimizu, T. Iwazaki, S. Nakagawa, M. Endo, M.S. Dresselhaus, Carbon 45 (2007) 2116–2125.
[16] A. Rudge, J. Davey, I. Raistrick, S. Gottesfeld, J. Power Sources 47 (1994) 89–107.
[17] S. Ghosh, O. Inganas, Adv. Mater. 11 (1999) 1214–1218.
[18] S.K. Mondal, K. Barai, N. Munichandraiah, Eelectrochim. Acta 52 (2007) 3258–3264.
[19] K. Wang, J.Y. Huang, Z.X. Wei, J. Phys. Chem. C 114 (2010) 8062–8067.
[20] M. Toupin, T. Brousse, D. Bélanger, Chem. Mater. 16 (2004) 3184–3190.
[21] T. Brezesinski, J. Wang, S.H. Tolbert, B. Dunn, Nat. Mater. 9 (2010) 146–151.
[22] K.W. Nam, K.B. Kim, J. Electrochem. Soc. 149 (2002) A346–A354.
[23] S.W. Lee, J. Kim, S. Chen, P.T. Hammond, Y. Shao-Horn, ACS Nano 7 (2010) 3889–3896.
[24] X.Y. Lang, A. Hirata, T. Fujita, M.W. Chen, Nat. Nanotechnol. 6 (2011) 232–236.
[25] B.E. Conway, V. Birss, J. Wojtowicz, J. Power Sources 66 (1997) 1–14.
[26] D. Li, J.X. Huang, R.B. Kaner, Acc. Chem. Res. 42 (2009) 135–145.
[27] S. Bhadra, D. Khastgir, N.K. Singha, J.H. Lee, Prog. Polym. Sci. 34 (2009) 783–810.
[28] M.X. Wan, Adv. Mater. 20 (2008) 2926–2932.
[29] J.X. Huang, R.B. Kaner, J. Am. Chem. Soc. 126 (2004) 851–855.
[30] D.W. Wang, F. Li, J.P. Zhao, W.C. Ren, Z.G. Chen, J. Tan, Z.S. Wu, L. Gentle, G.Q. Lu, H.M. Cheng, ACS Nano 3 (2009) 1745–1752.
[31] Q. Wu, Y.X. Xu, Z.Y. Yao, A. Liu, G.Q. Shi, ACS Nano 4 (2010) 1963–1970.
[32] J.J. Xu, K. Wang, S.Z. Zu, B.H. Han, Z.X. Wei, ACS Nano 4 (2010) 5019–5026.
[33] J. Erlebacher, M.J. Aziz, A. Karma, N. Dimitrov, K. Sieradzki, Nature 410 (2001) 450–453.
[34] L. Zhang, X.Y. Lang, A. Hirata, M.W. Chen, ACS Nano 5 (2011) 4407–4413.
[35] X.Y. Lang, L.H. Qian, P.F. Guan, J. Zi, M.W. Chen, Appl. Phys. Lett. 98 (2011) 093701.
[36] M. Baibarac, L. Mihut, G. Louarn, J.Y. Mevellec, J. Wery, S. Lefrant, I. Baltog, J. Raman Spectrosc. 30 (1999) 1105–1113.
[37] A.E. Fischer, M.P. Saunders, K.A. Pettigrew, D.R. Rolison, J.W. Long, J. Electrochem. Soc. 155 (2008) A246–A252.
[38] C.Z. Meng, C.H. Liu, L.Z. Chen, C.H. Hu, S.S. Fan, Nano Letters 10 (2010) 4025–4031.